Supplementary Material for " Optimal Ship-to-Grid Dispatch Considering Battery Thermal and Voltage Electrochemical-Thermal-Coupled Constraints"

Chao Lei, *Member, IEEE*, Shuangqi Li, *Member, IEEE*, and Yu Christine Chen, *Member, IEEE*

I. Derivations of (4a)

Substitute (1) into (2) and rearrange the resultant to yield

$$\widehat{T}^t_{i,j+1} = \Big(1 - \frac{h_{c,i}A_{s,i}\Delta h}{m_i C_{p,i}}\Big)T^t_{i,j} + \frac{\Delta h}{m_i C_{p,i}}(\epsilon H^{t+\Delta t}_{e,i} + h_{c,i}A_{s,i}T_{\text{amb}}), \quad \text{(I-1)}$$

where the variation of time-varying $H^t_{e,i}$ between time t and $t+\Delta t$ can be approximated by $\epsilon H^{t+\Delta t}_{e,i}$ with the constant coefficient ϵ set to 0.78. Further, substitute (1) into the corrector step in (3) to get

$$T^t_{i,j+1} = T^t_{i,j} + \frac{\Delta h}{2m_i C_{p,i}}(2\epsilon H^{t+\Delta t}_{e,i} + h_{c,i}A_{s,i}(2T_{\text{amb}} - T^t_{i,j} - \widehat{T}^t_{i,j+1})), \quad \text{(I-2)}$$

Next, substitute (I-1) into (I-2) to get

$$T^t_{i,j+1} = \omega_1 T^t_{i,j} + \omega_2 H^{t+\Delta t}_{e,i} + \omega_3, \quad j = 0, 1, 2, ..., n-1, \quad \text{(I-3)}$$

with ω_1, ω_2, and ω_3 as expressed in (4b)–(4d), respectively. The recurrence relation in (I-3) can be evaluated in closed form as

$$T^{t+\Delta t}_i = \omega_1^n T^t_i + \frac{1-\omega_1^{n-1}}{1-\omega_1}(\omega_2 H^{t+\Delta t}_{e,i} + \omega_3), \quad \text{(I-4)}$$

with boundary conditions $T^t_i = T^t_{i,0}$ and $T^{t+\Delta t}_i = T^t_{i,n}$.

II. Parameters of Approximate Cell Thermal and Voltage Constraints

In the case study, the approximate cell thermal constraint in M_3 [5] relates $T^{t+\Delta t}_i - T^t_i$ to either $p^t_{c,i}$ or $p^t_{d,i}$ and initial temperature T^0_i in the time period t. Thus, we can formulate the approximate cell thermal constraint as follows:

$$T^{t+\Delta t}_i = \begin{cases} T^t_i + e_0 + e_1 T^0_i + e_2 p^t_{c,i}, & \text{if } (\lambda_{\text{c}}, \lambda_{\text{d}}) = (1,0) \\ T^t_i + e_0 + e_3 T^0_i + e_4 p^t_{d,i}, & \text{if } (\lambda_{\text{c}}, \lambda_{\text{d}}) = (0,1) \end{cases} \quad \text{(II-5a)}$$

$$T^{t+\Delta t}_i \leqslant \overline{T}, \quad \text{(II-5b)}$$

where two sets of parameters $(e_0, e_1, e_2) = (0, 1, 2.3416)$ and $(e_0, e_3, e_4) = (0, 1, -2.5)$ are respectively fitted from the cell temperature surfaces for charging and discharging a batter cell as shown in Fig. 1(a) and (b) over a time period 15min, the initial cell temperature is assumed $T^t_i = T^0_i = 27$°C, and $\overline{T}$ denotes the maximum cell temperature limit.

In Fig. 2, the approximate hyperplane in yellow colour corresponding to γ_i is active below the cut line CD, otherwise the approximate hyperplane in pink colour is active. We also compare the errors in the simplified linear cell temperature constraint $T^t_i + e_0 + e_3 T^0_i + e_4 p^t_{d,i}$ in grey colour in Fig. 2. Via visual examination of Fig. 2, we observe that the cell temperature approximated by (4a) is very close to the surface yielded by the PDE solver. In fact, the maximum error in discharging mode is 1.8°C, acceptable for the optimal S2G dispatch. In contrast, the maximum cell temperature errors of simplified linear cell temperature constraint in grey color accounts for 4.1°C larger than those in our proposed approximate temperature calculations.

Moreover, the approximate cell voltage constraint in M_4 can be fitted from the the cell voltage surface as [6]

$$v^{t+\Delta t}_i = a_0 + a_1 p^t_{c,i} + a_2 S^t_i, \quad \text{(II-6a)}$$

$$v^{t+\Delta t}_i \leqslant \overline{v}, \quad \text{(II-6b)}$$

where parameters a_0, a_1, and a_2 are fitted from the cell voltage surface in the hyperplane in grey color as indicated in Fig. 7(b), and $\overline{v}$ denotes the maximum cell voltage limit. We provide the $a_0 = -23.1481$, $a_1 = -0.6551$, and $a_2 = -0.0278$ in case study in Section III. The line EF represents the upper bound of cell voltage profile, which obviously indicates (II-6b) can be inactive, thus preventing the cell from fully charging.

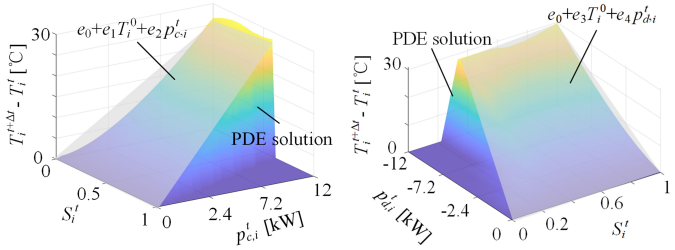

(a) (b)

Fig. 1. Approximate battery cell temperature $T^{t+\Delta t}_i - T^t_i$ during (a) charging, (b) discharging.

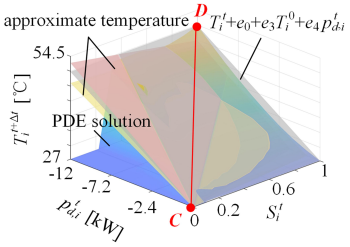

Fig. 2. Approximating battery cell temperature T^{t+1}_i during discharging.

III. Battery Cell Parameter Values

In this study, a BESS in ES_i consists of $N_i = 41$ $LiFePO_4$ battery modules arranged in series configuration, each with a capacity of 306.4 kWh. We select each battery cell capacity $I_{b,i} = 314$ Ah, nominal voltage $v_{\text{flat},i} = 3.4$ V with the operating voltage ranging from 2.5 V to 3.65 V, and current rate $C^t_{r,i} \in [0, \overline{C}_{r,i}]$ and $\overline{C}_{r,i} = 1.5$. For a battery cell, $\overline{p}_i \approx 3.65 \cdot 0.314 \cdot 1.5 \approx 1.7$ kW and $\overline{v} = 3.65$ V for a battery cell. Regarding thermal parameters, each battery cell has mass $m_i = 5.529$ kg and heat capacity $C_{p,i} = 1417.2\,\text{J}/(\text{kg}\cdot\text{K})$. The forced convection air cooling with four fans is available from four side openings of a battery cell with surface area $A_{\text{s},i} = 0.1271\,\text{m}^2$, and the heat transfer coefficient is $h_{c,i} = 5.0\,\text{W}/(\text{m}^2\cdot\text{K})$. Other parameters for electrochemical kinetics are given in Table I.

IV. Inaccurate Optimal S2G Dispatch for $S^t_i \geqslant S^t_{i,b}$

Consider cell voltage profiles of one battery cell at charging rates of 1.5C and 2.5C over a 900-second scheduling horizon, as shown in Fig. 3. In Fig. 3(a), t_A and t_B respectively represent the times at which the state of charge *should* reach 80% at charging rates of 2.5C and 1.5C (see points A and B respectively). However, in the case of the faster charging rate of 2.5C, charging terminates prematurely at t_C, but the resulting SoC is less than 80% (see point C). The premature termination is due to the cell reaching its maximum allowable voltage of $\overline{v} = 3.65$ V, marked as point D in Fig. 3(b). Here, the linear voltage profile plotted as the grey dashed trace in

TABLE I
PARAMETERS FOR ELECTROCHEMICAL KINETICS

Parameter	Negative electrode	Separator	Positive electrode
electrode plate area (m^2)	0.163	0.163	0.163
electrode thickness (m)	$78 \cdot 10^{-6}$	$20 \cdot 10^{-6}$	$45 \cdot 10^{-6}$
Li^+ diffusion coefficient (m^2/s)	$3.9 \cdot 10^{-5}$	-	$1.8 \cdot 10^{-8}$
active electrode volume fraction (%)	0.6	-	0.6
electrolyte phase volume fraction (%)	0.3	-	0.3
max solid phase concentration (mol/m^3)	31507	-	49000
particle radius (m)	$6 \cdot 10^{-6}$	-	$5 \cdot 10^{-6}$
reaction rate efficiency (A/m^2)	$9.77 \cdot 10^{-2}$	-	$1.19 \cdot 10^{-2}$
exchange current density of side reaction (A/m^2)	10	-	10
initial electrolyte concentration (mol/m^3)	$1.25 \cdot 10^4$	$1.25 \cdot 10^4$	$1.25 \cdot 10^4$
Binder volume fraction(%)	0.1	-	0.1
Separator volume fraction(%)	-	0.4	-

Fig. 3(b) underestimates the cell voltage at time t_C (see point E). In contrast, for the slower charging rate of 1.5C, the linear voltage profile suffices to approximate charging up to 80% SoC (see point F in Fig. 3(b)). The above demonstrates that the linear voltage model may not accurately capture the voltage profile even for SoC up to only 80%, which drastically limits the potential for ESs to serve as long-voyage transport.

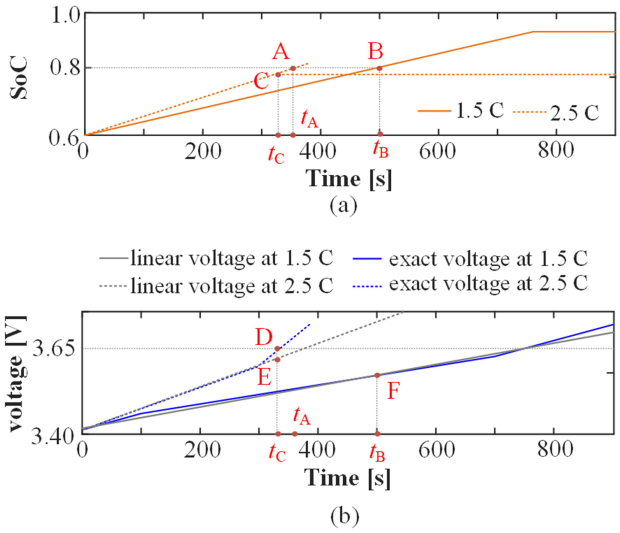

Fig. 3. Charging the battery cell with charging rates of 1.5C and 2.5C over 900s: comparing (a) SoC; and (b) voltage profile under the linear approximation and the exact model.